Microplasmas for direct, substrate-independent deposition of nanostructured metal oxides

Katherine E. Mackie,[1] Andrew C. Pebley,[2] Megan M. Butala[2], Jinping Zhang,[3] Galen D. Stucky,[1,2] Michael J. Gordon[4,a)]

[1]*Department of Chemistry and Biochemistry, University of California, Santa Barbara, Santa Barbara, CA 93106-9510, USA*

[2]*Materials Department, University of California, Santa Barbara, Santa Barbara, California 93106-5050, USA*

[3]*Platform for Characterization and Test, Suzhou Institute of Nano-Tech and Nano-Bionics, SINANO, Suzhou 215123, China*

[4]*Department of Chemical Engineering, University of California, Santa Barbara, Santa Barbara, CA 93106-5080, USA*

A general, substrate-independent method for plasma deposition of nanostructured, crystalline metal oxides is presented. The technique uses a flow-through, micro-hollow cathode plasma discharge (supersonic microplasma jet) with a 'remote' ring anode to deliver a highly-directed flux of growth species to the substrate. A diverse range of nanostructured materials (e.g., CuO, α-Fe_2O_3, and NiO) can be deposited on any room temperature surface, e.g., conductors, insulators, plastics, fibers, and patterned surfaces, in a conformal fashion. The effects of deposition conditions, substrate type, and patterning on film morphology, nanostructure and surface coverage are highlighted. The synthesis approach presented herein provides a general and tunable method to deposit a variety of functional and hierarchical metal oxide materials on many different surfaces. High surface area, conversion-type CuO electrodes for Li-ion batteries are demonstrated as a proof-of-concept example.

The ability to synthesize functional nanoscale materials, as well as to integrate these structures into devices, is fundamental for the development of next-generation micro- and optoelectronic devices, sensors, and energy harvesting and storage technologies [1-4]. Realization of nanomaterials and multi-scale systems often requires complicated processing steps that may involve a combination of wet chemistry, physical/chemical vapor deposition, vapor-liquid-solid or molecular beam epitaxy, self- and/or directed assembly, lithography, and etching. In addition, both wet and dry conditions, long processing times, high temperatures, vacuum processing, and templates or catalysts can be required. As such, we continually seek to develop general and tunable methods that can easily and rapidly create nanostructured functional materials. For example, atmospheric pressure plasmas [5,6], plasma sprays [7-9], and microplasmas [10-20] have shown much promise toward this goal. Extending and adapting such methods in a generic way to different material systems and deposition situations, as well as understanding how plasma operating conditions affect growth processes, is critical for their implementation.

In this work, we present a general, microplasma-based approach for direct deposition of nanostructured and conformal, crystalline metal oxides (CuO, NiO, α-Fe_2O_3) on virtually any substrate (e.g., conductors, insulators, polymers, fibers, patterns) at room temperature. A supersonic DC microplasma jet is seeded with organometallic precursors under oxidizing conditions to create a directed flux of growth species (e.g., atoms, ions, clusters, and/or nanoparticles) that are subsequently 'spray-deposited' onto the surface of interest. A remote, concentric ring anode, instead of the substrate, is used to complete the plasma circuit, allowing deposition on both conducting and insulting surfaces. Herein, we highlight the diverse range of materials that can be realized using microplasma growth and discuss how plasma operation and deposition conditions affect film morphology. High surface area CuO films were tested as conversion reaction anodes for Li-ion battery applications to demonstrate incorporation of microplasma-deposited films into devices, and the potential of microplasmas to synthesize nanostructured materials for energy applications.

Metal oxide nanostructures were deposited on a variety of different substrates using the microplasma deposition system depicted in Fig. 1. A flow-stabilized, direct-current hollow cathode discharge was used to crack sublimed organometallic precursors into active growth species (e.g., atoms, ions, and clusters), which were directed towards the substrate under supersonic flow conditions. Nickelocene, ferrocene, copper(II) acetylacetonate ($Cu(acac)_2$), and copper(II) hexafluoro-acetylacetonate hydrate ($Cu(hfac)_2$ xH_2O) (STREM) were sublimed and fed with 100-300 sccm Ar to the plasma jet cathode (stainless steel capillary, ID=500 μm) that was biased with current-regulated, DC high voltage (~10 mA, 300-800 V). A macor-insulated stainless steel ring near the capillary exit served as the anode to complete the plasma circuit. Oxygen (50-100 sccm) was introduced into the cathode gas feed or chamber background, the latter being maintained at 10-50 Torr. The substrate stage, 8-12 mm downstream from the capillary exit, was static or raster-scanned in a serpentine pattern at a rate of 2-10 μm/s during growth. Deposition rates varied for different materials, but generally fell in the 50-100 nm/minute range, measured directly beneath the jet centerline. Substrates were conducting (<0.001 ohm-cm) and insulating (>2000 ohm-cm) Si, glass coverslips, 300 nm ITO on glass, 50 μm Kapton polyimide film, 125 μm polished stainless steel, carbon paper, and fiberglass cloth. Deposition on patterned Si, i.e., micropillars created using colloidal lithography and reactive ion etching (see [21] for details), was also considered in order to evaluate if the deposited oxide films were conformal.

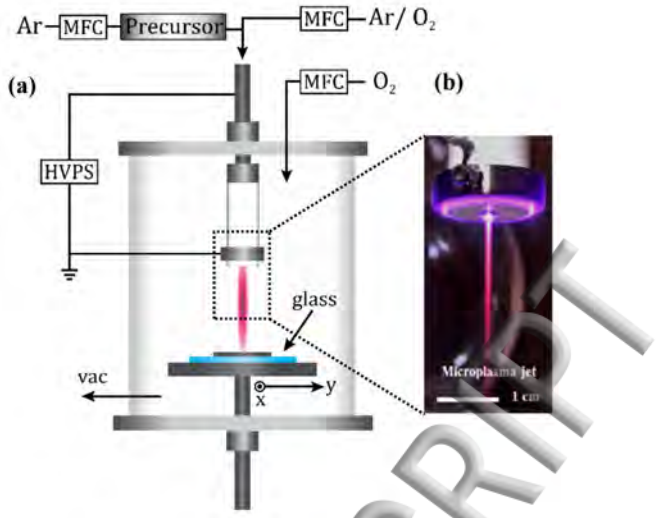

Figure 1: (a) Schematic of the microplasma deposition system. Ar carrier gas and sublimed organometallic precursor(s) are introduced into a stainless steel capillary (ID = 500 μm) inside a macor insulator with ring anode. A hollow cathode DC plasma is struck between the capillary and ring anode using a current-regulated, high voltage power supply (HVPS). O_2 is introduced into the chamber background at a rate of 50-100 sccm. (b) Photo of microplasma jet operating with 200 sccm Ar at 15 Torr and 8.5 mA. MFC = mass flow controller.

Crystallinity and phase of the deposited oxide coatings were analyzed via θ-2θ XRD (with -4° offset to suppress Si substrate peaks) using Cu Kα radiation on a PANalytical Empyrean diffractometer; high resolution micrographs and energy dispersive x-ray (EDX) spectra were taken on an FEI XL40 SEM and an FEI Tecnai G2 F20 S-Twin TEM using lacey carbon grids. X-ray photoelectron spectroscopy (XPS) analysis of the films was carried out on a Kratos Ultra system with monochromatic Al-Kα radiation. CuO films on Cu foil substrates were also tested as Li-ion battery electrodes that store charge by the conversion mechanism. Films were tested in Swagelok cells against a Li metal electrode in an electrolyte solution of 1 M $LiPF_6$ in 1:1 v/v ethylene carbonate:dimethyl carbonate with a glass filter paper separator. Cells were cycled at a rate of *C*/20, such that the theoretical $2e^-$ reaction of CuO to Cu and Li_2O upon reaction with Li takes place in 20 hours.

Nanostructured CuO was grown at room temperature on conducting, insulating, flexible, patterned, and fiber-based substrates to demonstrate the versatility of microplasma spray deposition (Fig. 2). Completing the plasma circuit through the remote anode ring, rather than the substrate, allowed deposition on insulating and floating substrates. All CuO deposits appeared to have similar agave-like 'nanowire' morphologies, and coatings were reasonably conformal on both fibers and Si micropillars. For the fiber-based substrates, complete conformal coverage of the oxide was observed on the first few layers of the material, with coverage becoming more sparse on the inner layers due to shadowing. XRD also showed that all of the coatings were the monoclinic (tenorite) phase of CuO. Several points about the CuO deposition are noteworthy, as discussed

in detail below: (1) films were nanocrystalline, monoclinic CuO with high surface area, even in the early stages of growth; (2) the identity and crystallinity of substrate do not appear to affect the film morphology; and (3) the deposited films were reasonably conformal.

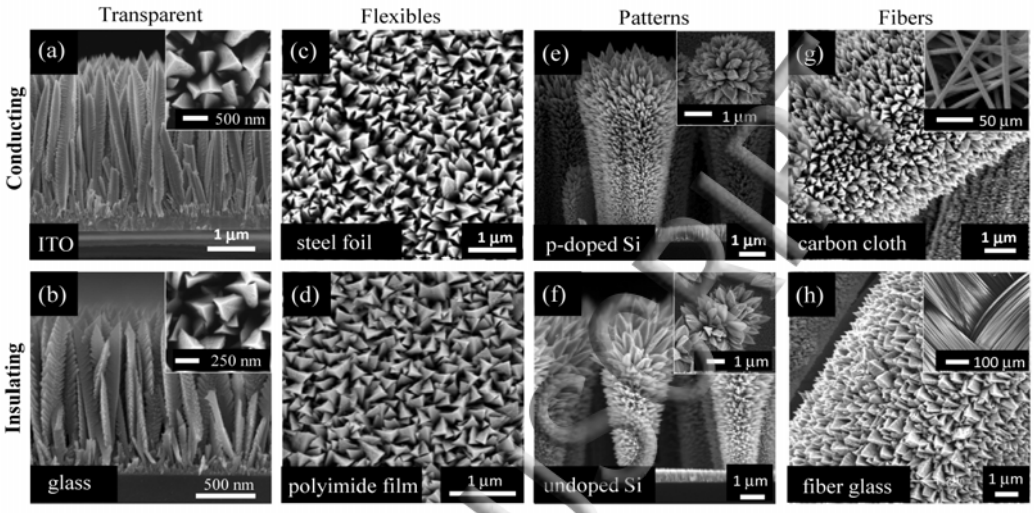

Figure 2: Microplasma spray deposition of CuO at 20 Torr, 8.5 mA with Ar:O_2 = 3:1 (O_2 in the background gas) on various, unheated substrates: (a) ITO, (b) glass, (c) stainless steel foil, (d) Kapton polyimide film, (e) conducting Si micropillars, (f) undoped (insulating) Si micropillars, (g) carbon paper, and (h) fiberglass cloth. Insets show top-down images of the oxide films at various length scales.

XRD of microplasma-grown CuO nanowires on various substrates revealed that the structures are crystalline (Fig. 3(a)), with no observable Cu_2O phase, and TEM further shows single-crystalline regions in the nanowires (Fig. 3(b)-(d)). Nanowires were seen to principally grow along the $[0\bar{2}0]$ direction. XPS analysis (see supplemental material [22]) also showed Cu^{2+} with characteristic CuO shakeup satellites, and no indication of Cu^0. Scherrer analysis of the (-111) and (111) reflections from the CuO nanowire sample estimates crystallite size at ~11 nm. The early stages of CuO growth were investigated by directing an Ar/$Cu(hfac)_2$ jet onto a lacey carbon TEM grid for one minute [Fig. 3(e)]. Although the plasma jet flow distorted the fragile lacey carbon grid, a conformal coating of small (< 5 nm), seed-like CuO crystal growths with facets can be seen. The corresponding SAED pattern [panel (f), inset] for this sample indicates that the seeds are indeed crystalline CuO, with reflections corresponding to the monoclinic tenorite phase. Contamination from the capillary tube cathode, ring anode, or C from the precursor, was not seen in the CuO films, as evidenced by the lack of EDX signals from stainless steel (Fe, Cr, Ni, etc.) and C. It is believed that active oxygen species are responsible for C removal from the growing film.

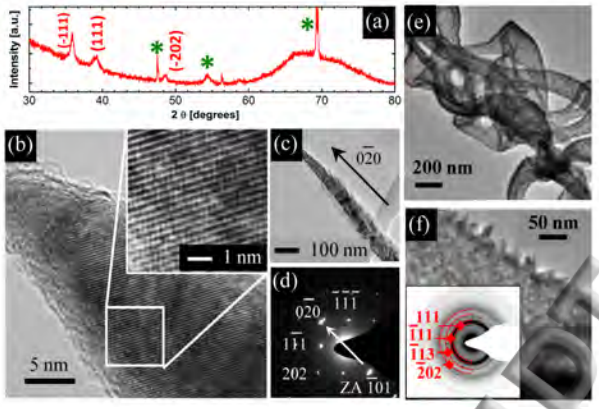

Figure 3: Characterization of microplasma-deposited CuO. (a) XRD scan of CuO deposit shown in Fig. 2(e), with reflections for monoclinic CuO (tenorite) shown. Green * are peaks from the Si substrate. (b) HRTEM image of a single-crystalline region of a CuO nanowire grown on Si with zoom of lattice planes. (c) Low resolution image and (d) SAED pattern of a CuO nanowire, showing growth along the $[0\bar{2}0]$ direction. (e) CuO nanocrystallites collected on a lacey carbon TEM grid exposed to an Ar/Cu(hfac)$_2$ jet for one minute. Panel (f) inset shows the SAED ring pattern with reflections for tenorite CuO noted.

It is initially surprising that crystalline CuO can be deposited on a substrate that is 'nominally' at room temperature (i.e., a thermocouple beneath the sample read <70 °C throughout deposition). However, particle nucleation and crystallization in non-thermal plasmas, with gas temperatures well below the crystallization threshold, have been reported and studied for several years [23-26]. These works suggest that, due to energetic surface processes (e.g., ion/electron collisions, ion-electron recombination, and chemical reactions), clusters (nanoparticles) in the plasma can be selectively heated above the overall gas temperature. For example, it has recently been estimated that Si nanoparticles <10 nm formed in a non-thermal atmospheric pressure microplasma can reach temperatures of 750K due to collisional heating [27]. A similar mechanism may be at play here, forming crystalline CuO seeds in the plasma; in addition, bombardment of the substrate by the plasma jet afterglow could enhance surface diffusion by locally increasing the surface temperature.

The microplasma deposition technique can also be easily extended to other oxide systems, such as NiO and α-Fe_2O_3, and for conformal deposition, as shown in Fig. 4. Similar plasma operating parameters (20 Torr, 8.5 mA, Ar:O_2=8:1 with O_2 in the jet) and static substrate were used to deposit both oxides on silicon micropillars at room temperature. Oxide coverage was reasonably conformal, with growth at the tops of pillars being favored due to shadowing effects. The observed crystal habits for each oxide were consistent with the bunsenite (rock-salt) phase of NiO and the hematite (rhombohedral) phase of α-Fe_2O_3. Scherrer analysis of the NiO (200) and Fe_2O_3 (104)/(110) reflections gave crystallite sizes of 20 and 23 nm,

respectively. XPS of the films (supplemental material [22]) additionally showed Fe^{3+} and Ni^{2+} chemical environments, in agreement with the Fe_2O_3 and NiO phases seen by XRD.

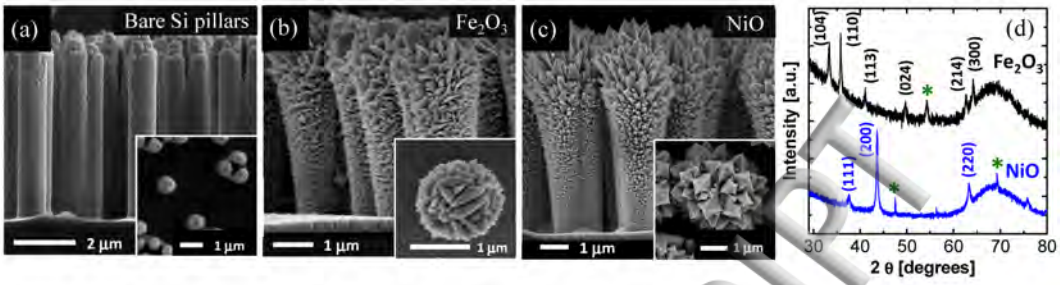

Figure 4: Microplasma deposition of (b) α-Fe_2O_3 and (c) NiO on 2.5 μm high Si micropillars (a). Insets show top-down zoom images of the oxide morphology. (d) XRD spectra of the films in (b) and (c). Reference reflections for NiO (bunsenite, rock-salt) and α-Fe_2O_3 (hematite, rhombohedral) are noted. Si substrate peaks are denoted with green *. All materials were deposited at 20 Torr, 8.5 mA with Ar:O_2 = 8:1 (O_2 in the jet) on unheated Si micropillar substrates; deposition time was 15 min with no substrate rastering.

Finally, nanostructured CuO films were evaluated as conversion electrodes for Li-ion batteries. CuO directly spray-deposited onto a copper foil current collector was assembled in a Swagelok cell against a Li metal anode at a rate of *C*/20. As can be seen in Fig.5, the microplasma-deposited electrode exhibited high specific capacity and good cyclability (~650 mA h/g over several charge-discharge cycles). The large and irreversible capacity loss after the first discharge-charge cycle is characteristic of CuO and other transition metal oxide conversion materials [28]. This loss is attributed to several factors including the incomplete conversion of Cu into Cu_2O instead of CuO during charge, cracking due to large volume expansion that could compromise electrical contact, and the formation of a solid electrolyte interphase (SEI) [28]. Despite the irreversible capacity loss in the first cycle, a capacity of about 650 mA h/g was retained over several cycles and is similar to capacities reported for CuO-based electrodes synthesized by traditional chemical methods [29-31]. The microplasma-deposited films have the added benefit in this application of not requiring the conductive carbon additives or polymer binders for electrode preparation, which can constitute 15% of the electrode film's mass. This preliminary result demonstrates both the ease of integrating microplasma-grown materials into devices with minimal processing, as well as the viability of microplasma deposition to synthesize materials for energy applications.

In this work, we demonstrated a simple, microplasma-based approach for direct, low temperature deposition of nanostructured metal oxides on a variety of substrates ranging from conductors to insulators, and polymer films to fibers. The films were highly crystalline and conformal, and raster scanning the substrate allowed deposition over larger areas with a single microplasma jet. Overall, we believe that microplasmas have great potential in materials processing, and deposition

methods can be extended to a wide range of functional materials and hybrid structures for use in micro- and optoelectronics, sensing, and energy applications.

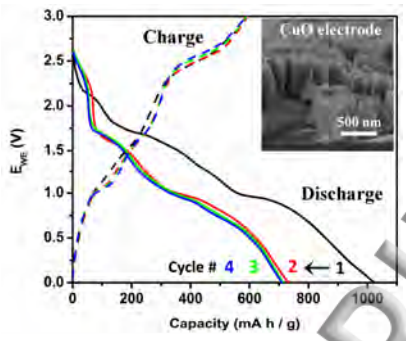

Figure 5: Discharge-charge profiles for microplasma-deposited CuO on Cu foil, used as a Li-ion battery anode. Testing configuration was a Swagelok cell operating at *C*/20 with 1M $LiPF_6$ in 1:1 v/v ethylene carbonate:dimethyl carbonate electrolyte and Li-metal cathode. (inset) SEM image of the CuO film.

This work was supported by the NSF PIRE-ECCI program (Advancing the US-China partnership in electron chemistry and catalysis at interfaces, Grant No. OISE 09-68399), leveraged equipment made possible by an NSF Career award (Grant No. CHE 0953441), and utilized MRL Shared Experimental Facilities supported by the MRSEC Program of the NSF under Award No. DMR 1121053; a member of the NSF-funded Materials Research Facilities Network (www.mrfn.org). K.E.M was supported by a PIRE-ECCI fellowship. The authors would also like to thank Federico Lora Gonzalez for Si micropillar substrates.

References

[1]X. Yu, T. J. Marks, and A. Facchetti, Nature Materials **15**, 383-396 (2016).

[2]C. Wang, L. Yin, L. Zhang, D. Xiang, and R. Gao, Sensors **10**, 2088-2106 (2010).

[3]J. Briscoe, and S. Dunn, Nano Energy **14**, 15-29 (2015).

[4]Z. Wang, and C. Liu, Nano Energy **11**, 277-293 (2015).

[5]D. Merche, N. Vandencasteele, and F. Reniers, Thin Solid Films **520**, 4219 (2012).

[6]H. Jung, J. Park, E.S. Yoo, G.-S. Han, H. S. Jung, M. J. Ko, S. Park, and W. Choe, Nanoscale **5**, 7825 (2013).

[7]R. Suryanarayanan, *Plasma spraying: theory and applications* (World Scientific, 1993).

[8]P. Fauchais, Journal of Physics D: Applied Physics **37**, R86 (2004).

[9]J. Karthikeyan, C. Berndt, J. Tikkanen, S. Reddy, and H. Herman, Materials Science and Engineering: A **238**, 275 (1997).

[10]D. Mariotti and R. M. Sankaran, Journal of Physics D: Applied Physics **43**, 323001 (2010).

[11]D. Mariotti and R. M. Sankaran, Journal of Physics D: Applied Physics **44**, 174023 (2011).

[12]T. L. Koh, E. C. O'Hara, and M. J. Gordon, Nanotechnology **23**, 425603 (2012).

[13]T. L. Koh, and M. J. Gordon, Journal of Vacuum Science and Technology A **31**, 061312 (2013)

[14]T. L. Koh, I. Chiles, and M. J. Gordon, Applied Physics Letters **103**, 163115 (2013).

[15]J. Kang, O. L. Li, and N. Saito, Nanoscale **5**, 6874 (2013).

[16]D. Mariotti, S. Mitra, and V. Svrcek, Nanoscale **5**, 1385 (2013).

[17]A. Kumar, P. A. Lin, A. Xue, B. Hao, Y. K. Yap, and R. M. Sankaran, Nature Communications **4** (2013).

[18]M. M. Rahman, I. Sultana, Z. Chen, M. Srikanth, L. H. Li, X. J. Dai, and Y. Chen, Nanoscale **7**, 13088 (2015).

[19]T. Koh, E. C. O'Hara, and M. J. Gordon, Journal of Crystal Growth **363**, 69 (2013).

[20]A. C. Pebley, A. Peek, T. M. Pollock, and M. J. Gordon, Chemistry of Materials **26**, 6026 (2014).

[21]F. L. Gonzalez, L. Chan, A. Berry, D. E. Morse, and M. J. Gordon, Journal of Vacuum Science & Technology B **32**, 051213 (2014).

[22]See supplemental material at [URL will be inserted by AIP] for XPS results.

[23]T. Lopez and L. Mangolini, Journal of Vacuum Science & Technology B **32**, 061802 (2014)

[24]L. Mangolini and U. Kortshagen, Physical Review E **79**, 026405 (2009).

[25]N. Kramer, E. Aydil, and U. Kortshagen, Journal of Physics D: Applied Physics **48**, 035205 (2015).

[26]H. Maurer and H. Kersten, Journal of Physics D: Applied Physics **44**, 174029 (2011).

[27]S. Askari, I. Levchenko, K. Ostrikov, P. Maguire, and D. Mariotti, Applied Physics Letters **104**, 163103 (2014).

[28]X. Wang, D.-M. Tang, H. Li, W. Yi, T. Zhai, Y. Bando, and D. Golberg, Chemical Communications **48**, 4812 (2012).

[29]S.-H. Park and W.-J. Lee, Scientific Reports **5** (2015).

[30]C. Wang, Q. Li, F. Wang, G. Xia, R. Liu, D. Li, N. Li, J. S. Spendelow, and G. Wu, ACS Applied Materials & Interfaces **6**, 1243 (2014).

[31]L. Wang, H. Gong, C. Wang, D. Wang, K. Tang, and Y. Qian, Nanoscale **4**, 6850 (2012).